ChemComm

COMMUNICATION

View Article Online
View Journal | View Issue

Cite this: *Chem. Commun.*, 2022, **58**, 13608

Received 28th September 2022,
Accepted 15th November 2022

DOI: 10.1039/d2cc05322e

rsc.li/chemcomm

Cinnamaldehyde hydrogenation over carbon supported molybdenum and tungsten carbide catalysts†

Marlene Führer, Tomas van Haasterecht and Johannes Hendrik Bitter *

The potential of carbon supported Mo and W carbides to replace Pt is shown for the hydrogenation of cinnamaldehyde. Although the carbide catalysts are 4–6 times less active, both the carbides and Pt are selective towards C═C hydrogenation. Unlike Pt, the carbides additionally form β-methylstyrene.

Since the 70s of the last century, it is clear that tungsten and molybdenum carbide based catalysts are potential alternatives to the scarce and expensive noble metal based catalysts (like Pt) for reactions that involve hydrogen activation.[1] Since then these metal carbides were investigated for use in many reactions like isomerisation, hydrodenitrogenation, syngas conversion and as electrocatalysts in fuel cells.[2,3] Later, the potential of molybdenum and tungsten carbide for biomass related conversions such as (hydro-)deoxygenation and dehydration to remove the oxygen of the biomass for the production of chemicals and biofuels (see ref. 4 and 5 for some reviews) has been shown. Recently, transition metal carbides have been applied for catalytic hydrogen transfer reactions.[6,7] In addition, some studies[8,9] show that tungsten carbide exhibits regioselectivity in hydrogenolysis. For instance, Fang *et al.*[9] showed high selectivity towards phenol when starting with guaiacol.

Though the above mentioned examples show the potential of molybdenum and tungsten carbides for hydrogenation as replacement for scarce noble metals like Pt, their potential for chemoselective hydrogenations has not been studied. These selective hydrogenations are often exemplified by cinnamaldehyde or crotonaldehyde hydrogenation towards either unsaturated alcohols or saturated aldehydes.[10–12]

The hydrogenation of α,β-unsaturated aldehydes like cinnamaldehyde is an important step toward valuable chemicals for the pharmaceutical, perfumery and flavour industries.[13,14] In addition, the hydrogenation of cinnamaldehyde has been widely used for a fundamental understanding in the investigation of chemo-selectivity in heterogeneous catalysis. Cinnamaldehyde can undergo C═C hydrogenation to yield hydrocinnamaldehyde (HCAL) and/or C═O hydrogenation to yield cinnamyl alcohol (COL) as illustrated in Scheme 1. Thermodynamically the hydrogenation of C═C is more favourable due to the lower bond energy of C═C.[10,15] Both HCAL and COL can be further hydrogenated to the saturated hydrocinnamyl alcohol (HCOL). Another possible pathway is the hydrogenolysis of COL into β-methylstyrene which can be further hydrogenated into propylbenzene. Propylbenzene can also be produced by the direct hydrogenolysis of HCOL.[16]

Noble metals with large d-bandwidth such as Pt or Ru have been widely used for the selective hydrogenation of CAL. They are highly active and their selectivity can be steered towards the C═O hydrogenation, as has been reviewed by Wang *et al.*[10] Different strategies for steering the selective have been reported like modifying the support,[18–20] adjusting the particle size/dispersion,[21–24] the addition of a second metal[25] or changing the reaction conditions (*e.g.* reaction medium[26,27]). Here we investigated the potential of carbon nanofiber (CNF) supported Mo and W carbide as an alternative catalysts for the hydrogenation of cinnamaldehyde.

Carbon nanofiber supported Mo and W carbides were synthesized by temperature programmed reduction as previously

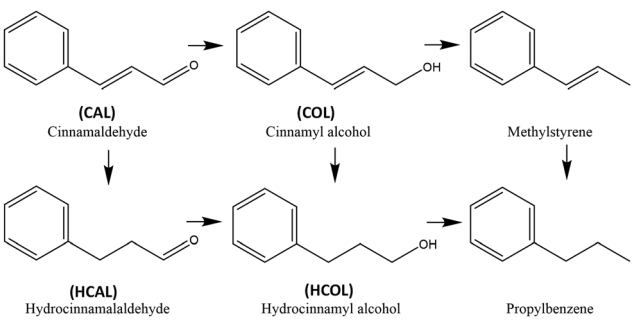

Scheme 1 Reaction scheme of the cinnamaldehyde hydrogenation.[16,17]

Department of Agrotechnology and Food Sciences, Wageningen University and Research, PO Box 17, 6700 AA Wageningen, The Netherlands.
E-mail: harry.bitter@wur.nl

† Electronic supplementary information (ESI) available. See DOI: https://doi.org/10.1039/d2cc05322e

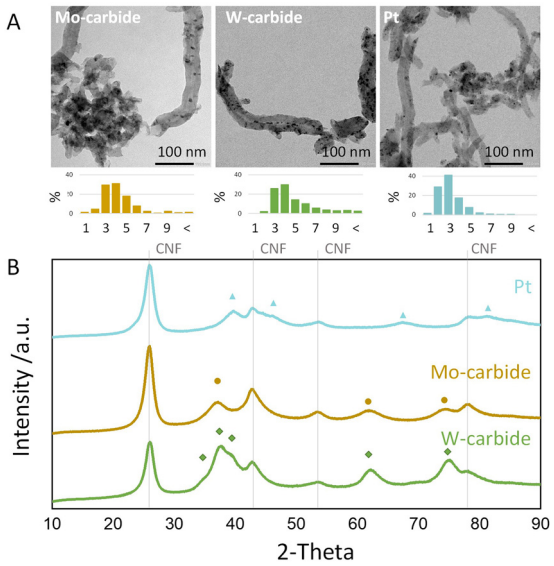

Fig. 1 (A) TEM images and (B) XRD pattern of the CNF supported Pt, Mo-carbide and W-carbide catalysts. ▲ metallic Pt, ● cubic α-MoC_{1-x} and ♦ hexagonal β-W_2C.

reported by Macedo *et al.*[28] In short, in house grown carbon nanofibers (using a Ni/SiO_2 growth catalyst and CO_2/H_2 at 550 °C as the carbon source) were oxidized with nitric acid and used as support.[29] These fibers were impregnated by incipient wetness using an aqueous solution of ammonium heptamolybdate or ammonium metatungstate. The obtained precatalyst was carburized at 650–700 °C in a mixture of 20% CH_4/H_2 for 2 h and afterwards directly used for the characterization (TEM, XRD, Chemisorption and XPS) or the hydrogenation reaction. For comparison, a carbon nanofiber supported Pt catalyst was prepared, by incipient wetness impregnation using an aqueous solution of $Pt(NH_3)_4(NO_3)_2$ followed by reduction at 300 °C under H_2 for 2 h (see ESI† for details of the catalyst preparation and characterization).

Fig. 1A displays representative TEM images and particle size distributions of the carbide and Pt catalysts. The average particle size for the carbide samples is between 3–4 nm and for the Pt samples around 2–3 nm. These images suggest that the carbide particles, as well as the metallic Pt, are well dispersed on the carbon support.

Fig. 1B shows the XRD patterns of the two carbide catalysts and the Pt catalyst. The signals at $2\theta = 28$ and $2\theta = 43°$ represent the (002) and (101) reflections of the CNF.[30] The reflections marked with the green diamond indicate the presence of the hexagonal β-W_2C phase (PDF 79-0743).[31] The Mo carbide sample shows reflections representing the cubic α-MoC_{1-x} phase (PDF 65-0280), marked with yellow dots.[28] The blue triangles indicated the characteristic metallic Pt crystal structure (PDF 88-2343).[32,33] TEM and XRD prove the successful synthesis of Pt and carbide nanoparticles with a particle sizes in a similar range.

CO chemisorption was used to establish the number of active sites as it is commonly used for Pt and carbide catalysts.[34,35] The carbide catalysts were carburized *in situ*, directly before the CO chemisorption to avoid any exposure to air. The Pt catalyst is activated in hydrogen prior to the CO chemisorption. Table 1 lists the CO chemisorption capacities of the freshly activated catalysts. It can be seen that the CO uptake for the Mo-carbide was around 67.5 μmol g^{-1} and that for the W-carbide was 20.4 μmol g^{-1}. For the Pt, a CO uptake of 58.1 μmol g^{-1} was measured. Thus, the CO uptakes for Pt and Mo-carbide are in a comparable range, while the W-carbide has a significantly lower CO uptake which indicates a higher concentration of potential active sites for Mo-carbide and Pt catalysts compared to the W-carbide catalyst.

Table 1 Hydrogenation of cinnamaldehyde (50 ml toluene, 13.6 g/l CAL, T = 200 °C, 20 bar H_2, 800 rpm), CO uptake and catalytic activity (TOF)

	Catalyst amount (mg)	Metal loading (wt%)	CO uptake (μmol g^{-1})[a]	TOF (min^{-1})[b]
Pt/CNF	100	5.0	58.1 ± 0.6	86
Mo/CNF	250	8.5	67.5 ± 1.3	14
W/CNF	250	15.0	20.4 ± 3.9	22

[a] Average of duplicate measurements. [b] TOF calculated at ~40% conversion.

The CAL hydrogen performance of the three catalysts was investigated in a gas-liquid batch reactor at 200 °C and 20 bar H_2. The reaction progress was assessed by periodically taking samples which were analysed by GC-FID. A detailed description of the experimental procedure can be found in the ESI† (catalytic hydrogenation). Fig. 2A shows the conversion of CAL over the three different catalysts as function of time. Clearly, the Pt catalyst shows the highest weight-based activity for the CAL hydrogenation among the different catalysts (full conversion within 1 h). For the Mo-carbide, full conversion was obtained within 5 hours while the W_2C catalyst only reached a maximum conversion of 95% after 7 h. In order to better compare the activity of the different catalysts also the turnover frequencies (TOF), based on the site density obtained from CO chemisorption, are given in Table 1. The Pt catalyst also has the highest TOF (86 min^{-1}) revealing about 4–6 times higher activity than the carbides, which show a very similar activity.

In order to understand the reaction pathway over the different catalysts, the normalized product distribution at selected conversion levels of X = 40% and X = 90% are given in Fig. 2B. The selectivity at 40% conversion shows that both Pt and the carbides favor the hydrogenation *via* the C=C bond, initially producing HCAL as main product. Subsequently, for all catalysts at higher conversion (X = 90%) the selectivity towards HCAL is decreased as it is further hydrogenated *via* C=O reduction resulting in increasing levels of HCOL. A closer inspection of HCAL selectivity at 90% conversion shows that Mo and W carbide catalysts still provide significantly higher selectivity of semi-hydrogenation product, HCAL (S = 40.9% and S = 43.0% respectively), than the Pt catalysts (S = 28.2%). Instead higher yields for the twice hydrogenated product, HCOL (S = 61.8%), were observed for the Pt catalysts. Thus, the further hydrogenation of the HCAL to HCOL is relatively

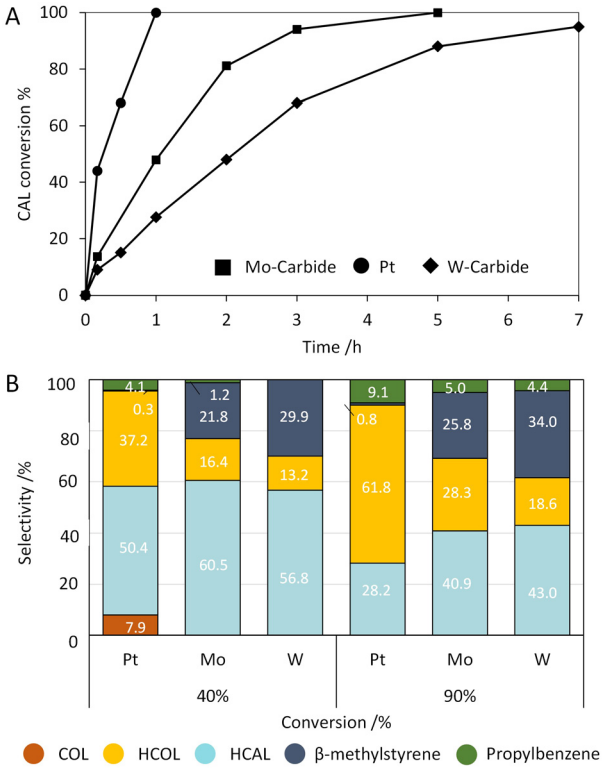

Fig. 2 (A) CAL conversion and (B) normalized product distribution at 40% and 90% conversion of CNF supported MoC_{1-x}, W_2C and Pt catalysts (50 ml toluene, 13.6 g per l CAL, T = 200 °C, 20 bar H_2, 800 rpm).

slower for the carbide catalysts than for the Pt catalysts. Besides C═C hydrogenation also C═O hydrogenation occurs over Pt as is evidenced by the presence of a minor amount of COL (S = 7.9%). Another striking difference is the observation that the carbide catalyst also produces β-methylstyrene, which is nearly absent with the Pt catalyst. The production of β-methylstyrene gives evidence that the carbide catalysts also follow the hydrogenation pathway *via* the COL. However, only trace amounts of COL were observed with the carbide catalysts, which leads to the suggestion that the C–O hydrogenolysis occurs fast (relative to C═O reduction) over the carbides. Unlike Pt, which shows only minor amounts of β-methylstyrene, the carbide catalysts thus also favour C–OH hydrogenolysis over C═C reduction. Finally, all catalysts also show some formation of the fully hydrogenated product propyl benzene, which in the case of Pt likely proceeds *via* hydrogenolysis of HCOL and in the case of the carbides could also proceed *via* β-methylstyrene.

The remarkable change in chemoselectivity between Pt based catalysts and carbide catalysts can be explained by the formation of acid sites on the carbide surface.[3,36] The brief exposure to ambient air during the transfer from the carburisation reactor to the hydrogenation vessel causes surface oxidation on the carbide surface, which was also observed by the XPS analysis (Fig. S1, ESI†).

A range of unidentified products could be detected during the hydrogenation with GC-FID especially for the W carbide catalyst (at long retention times, see chromatograms in Fig. S2 of ESI†). Further analysis with GC-MS revealed the formation of C18 coupling products. Additionally for W-carbide a substantial decrease in the carbon balance was noted (70% remaining) after 5 h of reaction, which reveals that for the W carbide some of the reactants are converted *via* side reactions, resulting in additional products that were not visible with GC-FID. For Pt and Mo-carbide the carbon balance remained in an acceptable range (90–95%, see Table S1, ESI†). These differences might be attributed to the acidic properties of the tungsten carbide surfaces, as is shown has previously been shown.[36]

The results above show that the carbide catalysts are 4–6 times less active than the Pt catalysts. However, considering the fact that transition metals are more abundant[37] and therefore less expensive than noble metals, the Mo-carbide are a viable non-noble alternative to Pt. Therefore, in the next step, we further investigated the effect of pressure and temperature on the activity and selectivity of the Mo-carbide catalyst.

The effect of pressure on the carbide catalyst activity was determined between 10–40 bar and is shown in Fig. S3 (ESI†). Going from 10 to 20 bar H_2 the reaction rate increases while going from 20 to 40 bar the H_2 pressure did not have an influence on the reaction rate. No clear effect of the pressure on the selectivity was observed.

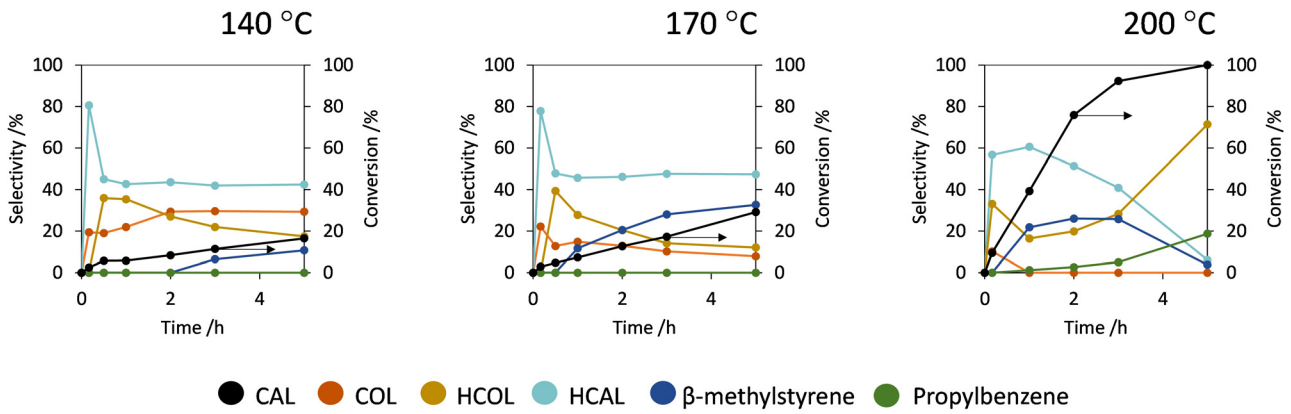

Fig. 3 CAL conversion and product yield of the Mo-carbide catalyst at 140, 170 and 200 °C (50 ml toluene, 13.6 g per l CAL, 20 bar H_2, 800 rpm).

Fig. 3 shows the influence of the temperature on the catalytic performance (selectivity and conversion) of Mo-carbide/CNF between 140–200 °C. By increasing the temperature from 140 °C to 170 °C the conversion increased from 19 to 30% after 5 h of reaction. Further increasing the temperature to 200 °C results in full conversion within 5 h. Fig. 3 also shows how the selectivity is affected by the temperature. It can be observed that at all temperatures HCAL is the dominant product at low conversion. This shows that the C=C hydrogenation is the main pathway at all temperatures. However, at lower reaction temperatures an increase in the selectivity towards COL can be observed. This can be attributed to a relatively larger decrease in the rate of C=C hydrogenation compared to the C=O hydrogenation as is evident from the increase in COL/HCAL ratio at low conversion with decreasing temperature (Fig. S4, ESI†). This indicates that the hydrogenation selectivity of Mo-carbide can be steered by changing the reaction temperature.

Finally, the stability of the Mo-carbide catalyst was assessed. Upon the first reuse, the catalyst activity decreased by about a factor 2 while this activity remained at this level for the third reused (see Fig. S5, ESI†). Metal leaching was determined by ICP analysis of the recovered reaction solution and found to be ~0.1% Mo (of the 8.5 wt%) after the first reaction. XRD characterisation (Fig. S6, ESI†) of the spent catalyst give no evidence for bulk oxidation, nor particle growth and therefore these are less likely deactivation mechanisms.

In conclusion, these findings demonstrate the potential of especially Mo-carbide catalysts for the hydrogenation of α,β-unsaturated aldehydes as alternative catalysts. The carbide catalysts and Pt, both favor the hydrogenation of the C=C bond to produce HCAL, although the carbides were less active. The main difference between Pt and the carbide was the high selectivity towards β methylstyrene with the carbide catalysts. Investigation of the effect of temperature for the Mo-carbide revealed a shift in selectivity towards the C=O hydrogenation product (COL) with decreasing temperature. These results highlight that the selectivity of the carbide catalysts can be steered by lowering the temperature. Investigation into how the properties of the catalysts (variation in support, particle size and crystal structure) influence the selectivity, as has already been shown for noble metal catalysts, is still needed for the carbide catalysts.

The research was financed by Dutch Research Council (NWO, 729.004.022). The authors thank Kai-Ching Fan (MSc student at Wageningen University) for the preliminary work which led to this article. We also thank Susan Witte for helping with the GC measurements, Barend van Lagen for the XPS measurements and Dmitry Pirgach for the ICP.

Conflicts of interest

There are no conflicts to declare.

Notes and references

1 R. B. Levy and M. Boudart, *Science*, 1973, **181**, 547–549.
2 E. Furimsky, *Appl. Catal., A*, 2003, **240**, 1–28.
3 M. M. Sullivan, C. J. Chen and A. Bhan, *Catal.: Sci. Technol.*, 2016, **6**, 602–616.
4 K. J. Smith, *Curr. Opin. Green Sustainable Chem.*, 2020, **22**, 47–53.
5 J. Pang, J. Sun, M. Zheng, H. Li, Y. Wang and T. Zhang, *Appl. Catal., B*, 2019, **254**, 510–522.
6 Z. Liu, X. Wang, X. Zou and X. Lu, *ChemistrySelect*, 2018, **3**, 5165–5168.
7 K. Wu, C. Yang, Y. Zhu, J. Wang, X. Wang, C. Liu, Y. Liu, H. Lu, B. Liang and Y. Li, *Ind. Eng. Chem. Res.*, 2019, **58**, 20270–20281.
8 H. Fang, A. Roldan, C. Tian, Y. Zheng, X. Duan, K. Chen, L. Ye, S. Leoni and Y. Yuan, *J. Catal.*, 2019, **369**, 283–295.
9 H. H. Fang, J. M. Du, C. C. Tian, J. W. Zheng, X. P. Duan, L. M. Ye and Y. Z. Yuan, *Chem. Commun.*, 2017, **53**, 10295–10298.
10 X. Wang, X. Liang, P. Geng and Q. Li, *ACS Catal.*, 2020, **10**, 2395–2412.
11 A. Dandekar and M. A. Vannice, *J. Catal.*, 1999, **183**, 344–354.
12 R. Zanella, C. Louis, S. Giorgio and R. Touroude, *J. Catal.*, 2004, **223**, 328–339.
13 S. S. Mohire and G. D. Yadav, *Ind. Eng. Chem. Res.*, 2018, **57**, 9083–9093.
14 D. Manikandan, D. Divakar and T. Sivakumar, *Catal. Commun.*, 2007, **8**, 1781–1786.
15 P. Gallezot and D. Richard, *Catal. Rev.*, 1998, **40**, 81–126.
16 A. Yepez, J. M. Hidalgo, A. Pineda, R. Černý, P. Jíša, A. Garcia, A. A. Romero and R. Luque, *Green Chem.*, 2015, **17**, 565–572.
17 J. Hájek, N. Kumar, P. Mäki-Arvela, T. Salmi, D. Y. Murzin, I. Paseka, T. Heikkilä, E. Laine, P. Laukkanen and J. Väyrynen, *Appl. Catal., A*, 2003, **251**, 385–396.
18 X. Zhang, Y. C. Guo, Z. C. Zhang, J. S. Gao and C. M. Xu, *J. Catal.*, 2012, **292**, 213–226.
19 M. L. Toebes, Y. Zhang, J. Hájek, T. A. Nijhuis, J. H. Bitter, A. J. Van Dillen, D. Y. Murzin, D. C. Koningsberger and K. P. de Jong, *J. Catal.*, 2004, **226**, 215–225.
20 H. Ma, L. Wang, L. Chen, C. Dong, W. Yu, T. Huang and Y. Qian, *Catal. Commun.*, 2007, **8**, 452–456.
21 F. Jiang, J. Cai, B. Liu, Y. Xu and X. Liu, *RSC Adv.*, 2016, **6**, 75541–75551.
22 H. Wei, C. Gomez, J. Liu, N. Guo, T. Wu, R. Lobo-Lapidus, C. L. Marshall, J. T. Miller and R. J. Meyer, *J. Catal.*, 2013, **298**, 18–26.
23 A. J. Plomp, H. Vuori, A. O. I. Krause, K. P. de Jong and J. H. Bitter, *Appl. Catal., A*, 2008, **351**, 9–15.
24 E. Bus, R. Prins and J. A. van Bokhoven, *Catal. Commun.*, 2007, **8**, 1397–1402.
25 W. Zhang, H. Xin, Y. Zhang, X. Jin, P. Wu, W. Xie and X. Li, *J. Catal.*, 2021, **395**, 375–386.
26 M. Chatterjee, F. Zhao and Y. Ikushima, *Appl. Catal., A*, 2004, **262**, 93–100.
27 H. Wang, B. Liu, F. Liu, Y. Wang, X. Lan, S. Wang, B. Ali and T. Wang, *ACS Sustainable Chem. Eng.*, 2020, **8**, 8195–8205.
28 L. S. Macedo, D. R. Stellwagen, V. T. da Silva and J. H. Bitter, *ChemCatChem*, 2015, **7**, 2816–2823.
29 K. P. De Jong and J. W. Geus, *Catal. Rev.*, 2000, **42**, 481–510.
30 A. L. Jongerius, R. W. Gosselink, J. Dijkstra, J. H. Bitter, P. C. A. Bruijnincx and B. M. Weckhuysen, *ChemCatChem*, 2013, **5**, 2964–2972.
31 R. A. Mitran, M. C. Radulescu, L. Buhalteanu, L. C. Tanase, D. G. Dumitrescu and C. Matei, *J. Alloys Compd.*, 2016, **682**, 679–685.
32 T. Hyde, *Platinum Met. Rev.*, 2008, **52**, 129–130.
33 M. Führer, T. van Haasterecht, N. Masoud, D. H. Barrett, T. Verhoeven, E. Hensen, M. Tromp, C. B. Rodella and H. Bitter, *ChemCatChem*, 2022, **14**(19), e202200493.
34 P. A. Aegerter, W. W. C. Quigley, G. J. Simpson, D. D. Ziegler, J. W. Logan, K. R. McCrea, S. Glazier and M. E. Bussell, *J. Catal.*, 1996, **164**, 109–121.
35 S. Oyama, *Catal. Today*, 1992, **15**, 179–200.
36 D. R. Stellwagen and J. H. Bitter, *Green Chem.*, 2015, **17**, 582–593.
37 R. M. Bullock, J. G. Chen, L. Gagliardi, P. J. Chirik, O. K. Farha, C. H. Hendon, C. W. Jones, J. A. Keith, J. Klosin and S. D. Minteer, *Science*, 2020, **369**, eabc3183.